Electronic Supplementary Information
for the
Electrocatalytic Water Oxidation by Cu^{II} Complexes with Branched Peptides

József S. Pap,[a,*] Łukasz Szyrwiel,[b,c,*] Dávid Srankó,[a] Zsolt Kerner,[a] Bartosz Setner,[b] Zbigniew Szewczuk,[b] Wiesław Malinka[d]

[a]MTA Centre for Energy Research, Surface Chemistry and Catalysis Department, P.O. Box 49, H-1525 Budapest, Hungary

[b]Faculty of Chemistry, University of Wrocław, ul. F. Joliot-Curie 14, 50−383 Wrocław, Poland

[c]CNRS/UPPA, LCABIE, UMR5254, Helioparc, 2, av. Pr. Angot, F-64053 Pau, France

[d]Department of Chemistry of Drugs, Wrocław Medical University, ul. Borowska 211, 50-552 Wrocław, Poland

List of contents:

Syntheses. The synthetic processes of 3G and 2GH, their complexation properties with Cu are discussed elsewhere, as well as detailed spectroscopic characterization (UV/VIS, CD, EPR and ESI-MS) of the different pH-dependent species (ref. 15 in the main text).

Electrochemistry. Cyclic voltammetry (CV), square-wave voltammetry (SWV) and controlled potential electrolysis (CPE) measurements were performed on a general purpose potentiostat (BioLogic SP-150) equipped with a low-current unit. A standard three-electrode setup was used including a glassy carbon (0.07 cm^2, for CV and SWV), or indium-tin-oxide (ITO, ~0.7 cm^2, for CPE) working electrode, Pt auxiliary electrode (~7 cm^2) and Ag/AgCl (3 M KCl, 0.2 V *vs.* SHE) reference electrode. The cell was equipped with a pH microelectrode (Mettler-Toledo) and a fluorescent O_2 sensor (Ocean Optics NeoFox). The GC working electrode was carefully rinsed, polished and rinsed again right before use. The cell was kept under argon throughout the SWV measurements, while electrocatalytic tests were run either under air, or argon, but no difference was experienced in catalysis. All salts were purchased from commercial sources and were of puriss p.a. grade. The complex solutions were made before the experiments using slight excess of ligands (0.9:1 Cu to ligand ratio), these solutions were then mixed with appropriate amounts of phosphate buffer and titrated with 1N NaOH to the wished pH.

The $Cu^{III/II}$ formal potentials ($E°'$) were determined from pH-dependent SWV in a ~2.5 pH range from above 9 for **1** and **2**. In this range the $Cu^{II}H_{-2}L$ forms are predominant. We applied SWV instead of CV to follow the changes in the $E°'$ values accurately, upon shifting the pH by small increments. In SWV the current difference (I_{net}) between a forward (I_{for}) and reverse (I_{rev}) pulse polarization is plotted against potential, therefore this technique is highly discriminating against background currents. Moreover, the short duration of concomitant oxidative and reductive pulses (20-40 ms) was sufficient to reach reversibility, thus E_{net} (potential of I_{net}) can be directly associated with $E°'$ (for further details of this method and applications see refs.: B. W. Berry, M. C. Martínez-Rivera, C. Tommos, *Proc. Natl. Acad. Sci. USA*, 2010, **109**, 9739; F. Scholz (Ed.), *Electroanalytical Methods*, 2010, Springer-Verlag, Berlin; A.B. Miles, R.G. Compton, *J. Phys. Chem. B*, 2000, **104**, 5331; P. Wardman, *J. Phys. Chem. Ref. Data*, 1989, **18**, 1637). Tables S1 and S2 sum the measured data for the curves in Fig. 1 and Fig. S1.

X-ray photoelectron spectroscopy (XPS). Surface analysis of Cu was performed by XPS on a KRATOS XSAM 800 XPS machine equipped with an atmospheric reaction chamber. Al Kα characteristic X-ray line, 40 eV pass energy and FAT mode were applied for recording the XPS lines of full binding energy spectra of ITO surfaces before and after use with Cu-peptide or cupric salt.

UV/VIS spectroscopy. Electronic absorption spectra were taken between 400 and 700 nm, with an Agilent Cary 60 spectrophotometer equipped with a 1 cm path length fiber optic probe that could be directly used in the electrochemistry cell.

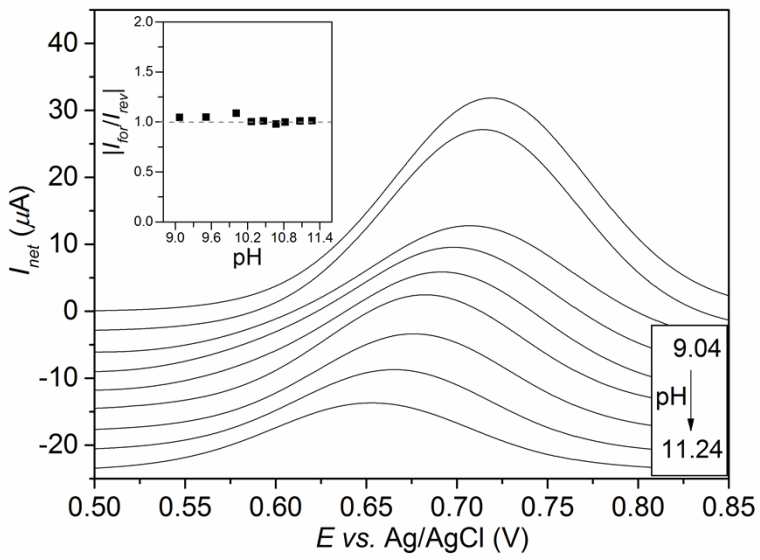

Figure S1. Variation of SW voltammograms with pH of a freshly prepared Cu:3G = 0.9:1 solution. Conditions: [Cu] = 0.32 mM, 0.1 M $NaClO_4$ electrolyte, titrated with NaOH, 25°C, under Ar, P_H = 50 mV, f = 25 Hz, S_H = 0.2 mV. The insert shows the ratio of the forward (oxidation) and reverse (reduction) current peak component. Insert: the ratios approximating 1 are indicative of reversibility.

Table S1. Formal potentials determined from SWV for the $Cu^{III/II}$ redox transition of **1** at different pH values.

pH	$E°'(Cu^{III/II})$ *vs.* Ag/AgCl (V)[a,b]	$\lvert I_{for}/I_{red} \rvert$
9.07	0.717(2)	1.05
9.51	0.714(2)	1.05
10.01	0.706(3)	1.09
10.26	0.699(3)	1.01
10.46	0.691(3)	1.01
10.67	0.682(2)	0.98
10.82	0.676(2)	1.00
11.07	0.665(2)	1.01
11.27	0.654(2)	1.01

[a]error in last digit is indicated in parenthesis

[b]to obtain values against SHE 0.2 V has to be added to the measured values against the Ag/AgCl ref. electrode.

Table S2. Formal potentials determined from SWV for the $Cu^{III/II}$ redox transition of **2** at different pH values.

pH	$E°'(Cu^{III/II})$ *vs.* Ag/AgCl (V)[a,b]	$\lvert I_{for}/I_{red} \rvert$
9.34	0.738(3)	1.03
9.68	0.725(3)	0.94
9.92	0.718(3)	1.00
10.14	0.708(3)	0.95
10.34	0.699(3)	1.00
10.56	0.683(3)	1.02
10.74	0.672(3)	0.96
10.89	0.665(3)	0.95
11.08	0.652(3)	0.97
11.30	0.639(3)	0.96

[a]error in last digit is indicated in parenthesis

[b]to obtain values against SHE 0.2 V has to be added to the measured values against the Ag/AgCl ref. electrode.

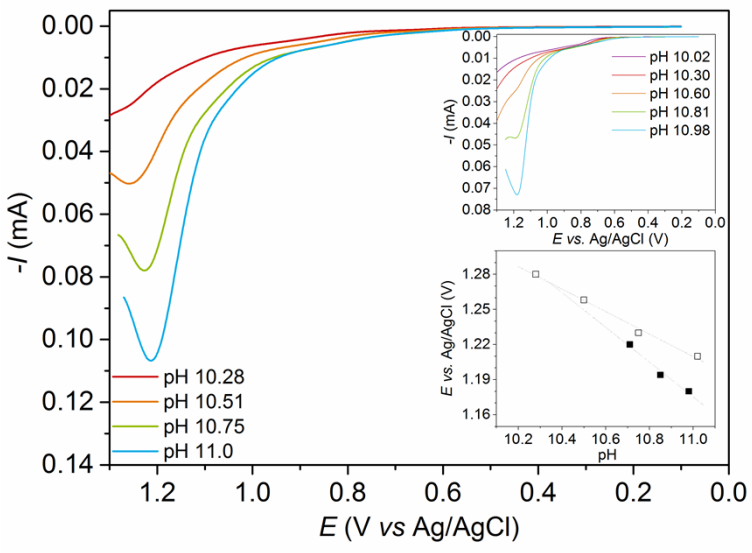

Figure S2. Effect of pH on the build-up of the catalytic current peak (I_{cat}) and potential (E_{cat}) for **1** (0.5 mM in 0.15 M phosphate buffer, 25°C, GCE, ν = 20 mVs^{-1}). Inserts: the same plot for **2** (0.2 mM) among identical conditions (top), dependence of E_{cat} on pH (dashed lines are fitted linears and only serve as guide for the eye). Only current responses on forward polarization were plotted for better visual.

Table S3. Comparison of the catalytic current peaks in the presence of **1** and **2** (data for Fig. 3, I_{cat} is given in μA, scan rate = 5 mV/s, phosphate buffer concentration is 0.15 M, t = 25°C, pH = 11).

[Cu] (mM)	**1**	**2**
0.14		34
0.31		76
0.40		100
0.48		119
0.54		132
0.65		159
0.21	37	
0.30	48	
0.50	90	
0.65	118	

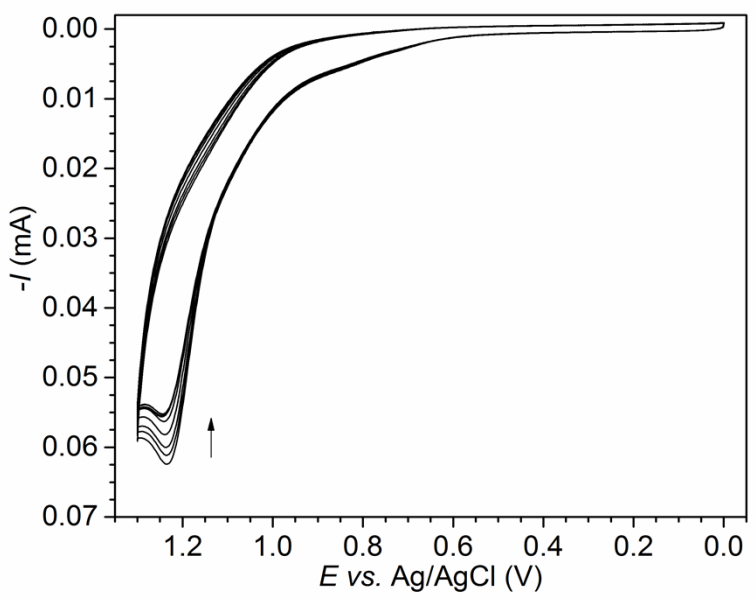

Figure S3. Multiple scans (10) CV experiment on a 0.2 mM solution of **2** in 0.15 M phosphate buffer at 40 mVs^{-1} at a GCE. The last five scans are overlapping.

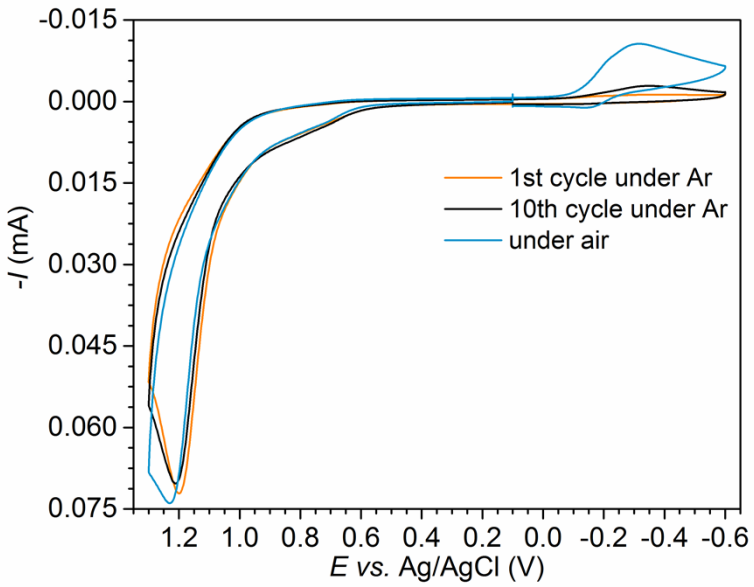

Figure S4. Experiments aiming detection of O_2 reduction upon cathodic polarization of GCE in a ~0.2 mM solution of **2** in 0.15 M phosphate buffer. Electrodes were first polarized to the anodic direction to 1.3 V, then to -0.6 V on the reverse direction. The wave typical for O_2 reduction increased with the number of scans. Note that gas bubbles were observed at the GCE after multiple cycles.

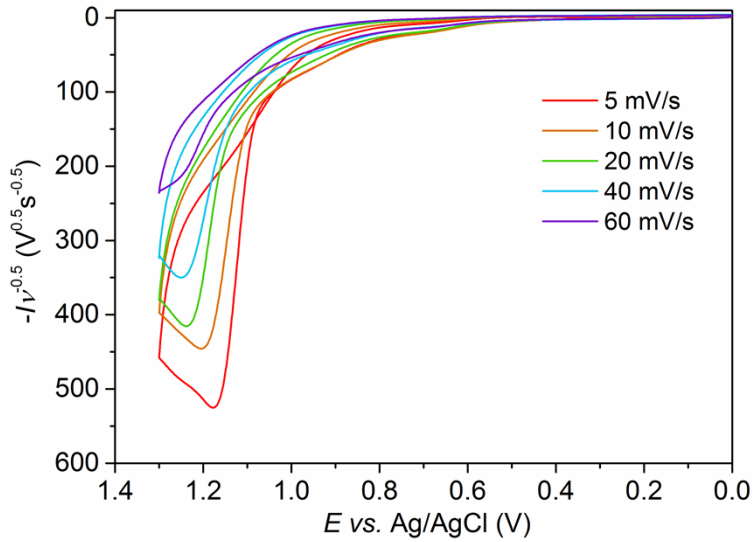

Figure S5. Catalytic current responses of **1** (0.2 mM, 0.15 M phosphate buffer, pH = 11, 25°C) normalized with $\nu^{0.5}$.

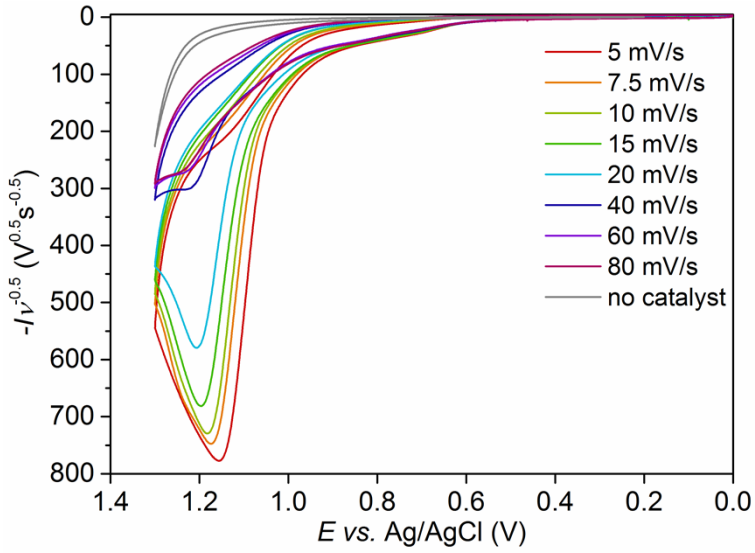

Figure S6. Catalytic current responses of **2** (0.2 mM, 0.15 M phosphate buffer, pH = 11, 25°C) normalized with $\nu^{0.5}$. CV in grey: rinsed, but not polished electrode after experiments transferred into fresh buffer.

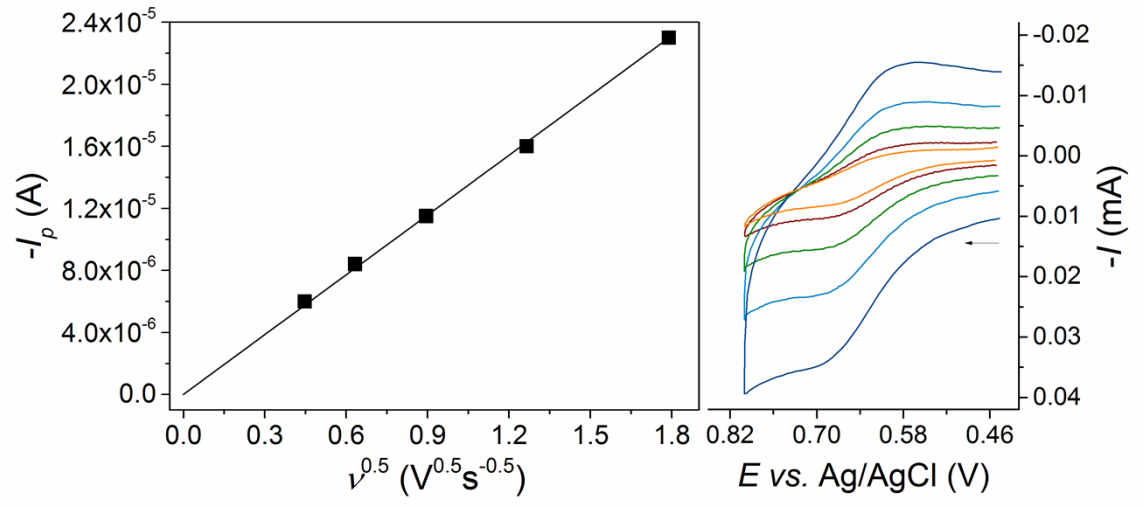

Figure S7. *Right*: cyclic voltammetry among catalytic conditions, [Cu] = 0.5mM, c(buffer) = 0.15 M, *t* = 298 K, A = 0.07 cm^2 GC electrode, pH = 11, scan rates of 200, 400, 800, 1600 and 3200 mVs^{-1}. *Left*: the oxidation peak current (I_p) plotted against the square root of scan rate (ν). *D* was determined from equation: $I_p = 0.446nFA[Cu](nF/RT)^{0.5}D^{0.5}\nu^{0.5}$.

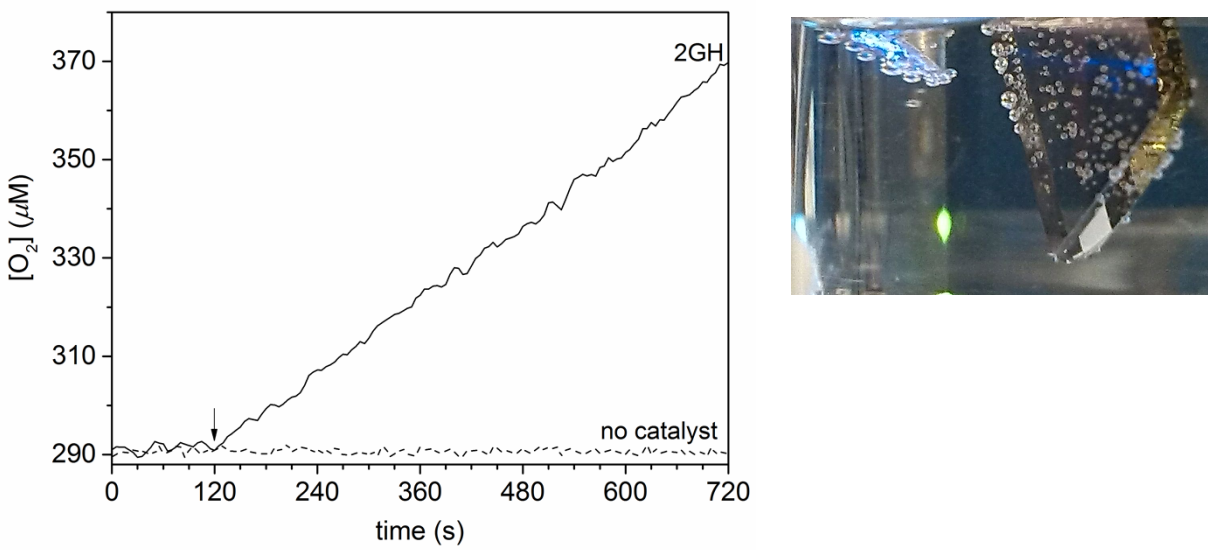

Figure S8. Initial oxygen evolution during controlled potential electrolysis at 1.1 V *vs.* Ag/AgCl, followed in a thermostated electrochemical cell equipped with a calibrated fluorescence probe (Ocean Optics NeoFox) in the presence or absence of 0.5 mM **2** at pH = 11 (0.15 M phosphate buffer, under air). Controlled potential electrolysis was started at 120 s in a stirred solution. Working electrode: 0.7 cm^2 ITO, auxiliary electrode: Pt (~7 cm^2). The photo illustrates that gas bubbles were developed at surfaces after considerable oversaturation of the solution with O_2.

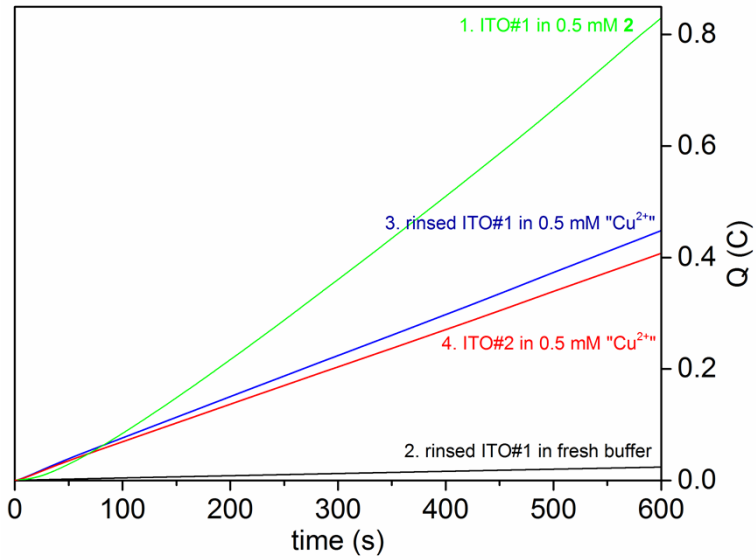

Figure S9. First 10 minutes of CPE at 1.1 V on ITO (~0.7 cm^2). The numbers indicate the order of tests. Test number 1 corresponds to the test shown in Fig. S8.

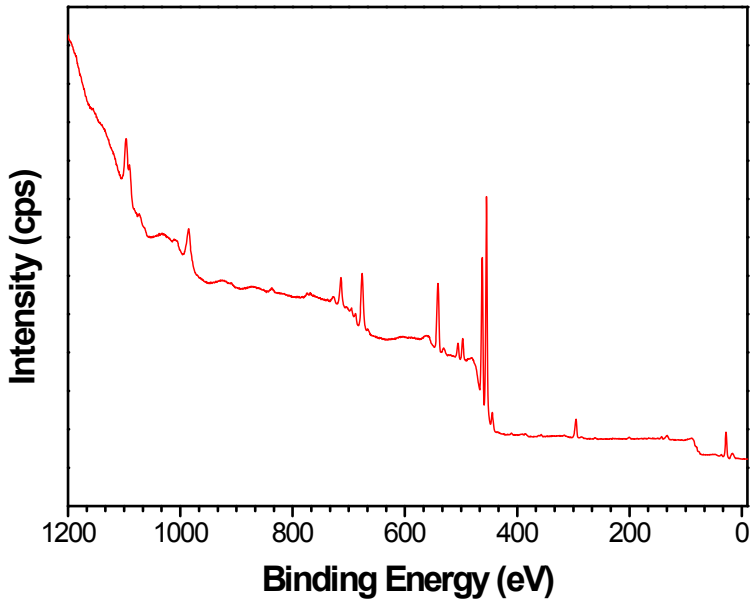

Figure S10. XPS spectrum of a new ITO surface.

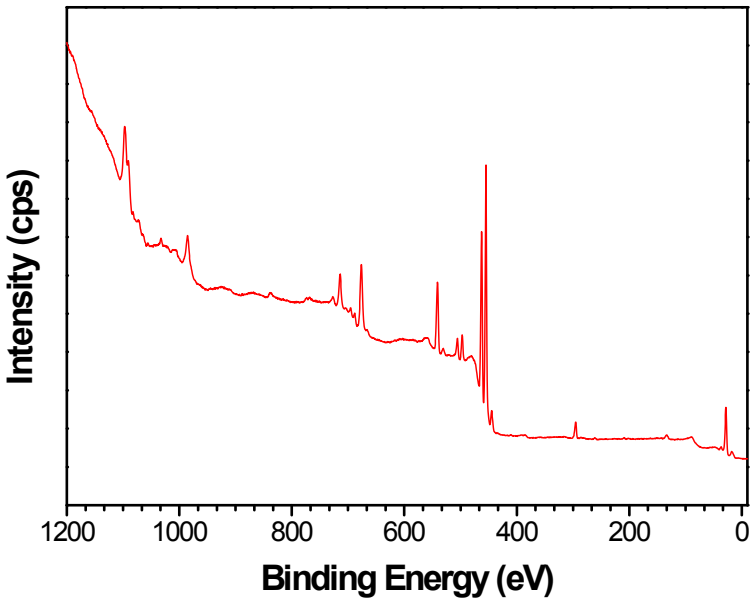

Figure S11. XPS spectrum of rinsed ITO after CPE at 1.1 V vs. Ag/AgCl for 90 minutes in presence of 0.5 mM **2** in a pH 11 phosphate buffer (ITO#1 from Fig. S9 after test 1).

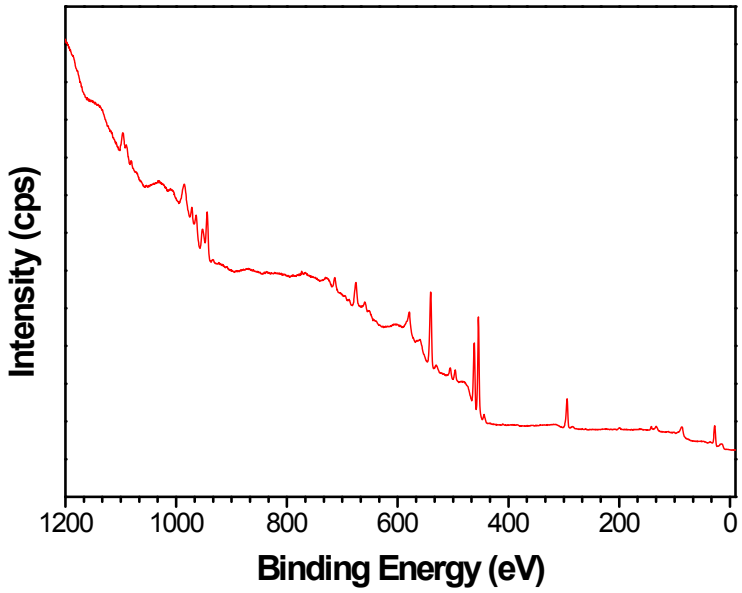

Figure S12. XPS spectrum of an ITO surface after 30 minutes of CPE at 1.1 V (ITO#2 after test 4 in Fig. S9). The four-band pattern is typical to CuO and $Cu(OH)_2$ type layers. The relative to the overall elements ratio for CuO is 5.72 At% (from Cu 2p at 933.9 eV) and 2.74 At% for $Cu(OH)_2$ (from Cu 2p at 935.9 eV).

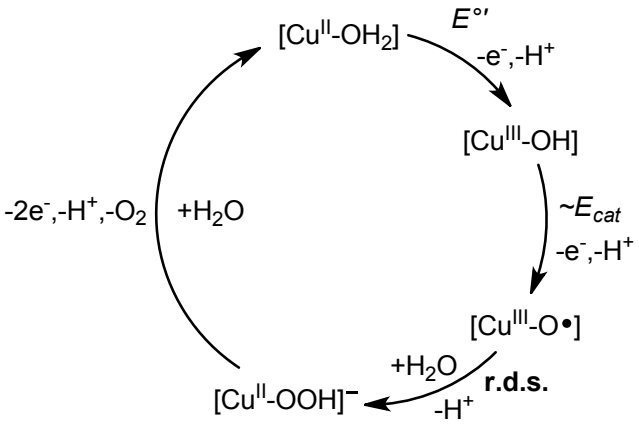

Scheme S1. Proposed mechanism for the electrocatalytic water oxidation by **1** and **2** (analogously to the mechanism proposed by Meyer *et al.*). Ligand $H_{-2}L$ is omitted from the formula. In the first step the oxidation of **1**(**2**) to $\mathbf{1}^{ox}(\mathbf{2}^{ox})$-$H^+$ takes place (at $E°'$ as denoted in the scheme). This is followed by a second oxidation to a proposed $[Cu^{III}\text{-}O\bullet]$ intermediate (at $\sim E_{cat}$). This oxyl radical reacts with H_2O in the rate determining step (**r.d.s.**) to form the O-O bond and the intermediate Cu^{II}-peroxide is readily oxidized at the E_{cat} potential (possibly to $[Cu^{III}\text{-}OO\bullet]$) enhancing the current and finally releasing O_2 and coordinating a next water molecule thus re-entering the catalytic cycle. The acceleration of catalysis by the equatorial His imidazole ligand of **2** can be associated with a number of effects. Most importantly, it can directly result in cation π-interaction with protons released in PCET processes.

This effect is known in enzyme catalysis. Spin delocalization over the imidazole moiety in the case of intermediate radical would be also an option. Indirectly, due to its higher affinity to Cu^{II}, His excludes a terminal amino group from the coordination sphere that in turn can act as internal proton acceptor to promote PCET processes.